J Mater Sci: Mater Electron (2011) 22:228–232
DOI 10.1007/s10854-010-0119-6

Structural, spectroscopic and microwave characterizations of $(Sm_{0.5}Y_{0.5})Ti(Nb_{1-x}Ta_x)O_6$ ceramics

James T. Joseph · Shyla Joseph · Annamma John · J. K. Thomas · V. S. Prasad · Sam Solomon

Received: 3 March 2010 / Accepted: 7 April 2010 / Published online: 17 April 2010

Abstract Microwave dielectric ceramics of the type $(Sm_{0.5}Y_{0.5})Ti(Nb_{1-x}Ta_x)O_6$ were prepared for $x = 0$, 0.2, 0.4, 0.6, 0.8 and 1 through the conventional solid state ceramic route. The ball-milled compositions were calcined at 1,250 °C. The cylindrical pellets were sintered at temperatures between 1,385 and 1,450 °C. The densities were determined by Archimedes method. The structure was analyzed using X-ray diffraction method. The microwave dielectric properties of the polished pellets were measured using cavity resonator method. The morphological studies were done using Scanning Electron Microscopy and Transmission Electron Microscopy. The Raman spectra were recorded and analyzed to confirm the structural change. The photoluminescence spectra were also taken and the emission lines were identified. A correlation study was done among the measured properties and parameters. Most of the samples have high dielectric constant, high quality factor and low temperature coefficient of resonant frequency and hence suitable for microwave applications.

J. T. Joseph
Department of Chemistry, St. John's College, Anchal 691 306, Kerala, India

S. Joseph · A. John · S. Solomon (✉)
Department of Physics, St. John's College, Anchal 691 306, Kerala, India
e-mail: samdmrl@yahoo.com

J. K. Thomas
Department of Physics, Mar Ivanios College, Thiruvananthapuram 695 015, Kerala, India

V. S. Prasad
Materials and Minerals Division, National Institute for Interdisciplinary Science and Technology, Thiruvananthapuram 695 019, Kerala, India

1 Introduction

The discovery and use of dielectric materials as resonators in wireless communication devices started since the work of Richtmyer in 1939 [1]. The metallic cavity resonators have been replaced by dielectric resonators due to their compactness, high thermal stability, high efficiency and low cost of production [2]. The essential requirements of a material to be used as dielectric resonator are high permittivity ($\varepsilon_r > 20$), high unloaded quality factor ($Q_u >$ 1,000 GHz) and low temperature coefficient of resonant frequency ($\tau_f < 20$ ppm/K). Dielectric resonators are commonly used to design filters, oscillators, antennas etc. in wireless communication devices. A dielectric resonator with the desirable properties can create and filter frequencies in oscillators with maximum thermal stability. Dielectric resonators having dielectric constant in the range 25–50 are used for satellite communication devices and in cell phone base stations while those with higher dielectric constant are required for the application in mobile phones. A large number of materials are already reported that satisfy one or more of the essential conditions required for their use as dielectric resonators [3–12].

According to Sebastian et al., $SmTiNbO_6$ crystallize in the orthorhombic aeschynite structure with positive τ_f value (+46 ppm/K) while $YTiNbO_6$ crystallize with orthorhombic euxenite structure with a negative τ_f value (−45 ppm/K) [13]. Thus, a ceramic of the formula $(Sm_{0.5}Y_{0.5})TiNbO_6$ is expected to give a low τ_f value. According to Surendran et al. [14] $RETiTaO_6$ system gives a lower τ_f value in

comparison with the corresponding $RETiNbO_6$ systems. Hence, expecting τ_f values closer to zero, we have substituted Ta for Nb. In this paper we report the preparation and microwave, vibrational and optical characterizations of $(Sm_{0.5}Y_{0.5})Ti(Nb_{1-x}Ta_x)O_6$ (XTa_x) ceramics.

2 Experimental

The ceramic samples are prepared by conventional solid state ceramic route. Lanthanide oxides (CDH 99.9%), Nb_2O_5 and Ta_2O_5 (NFC 99.9%) were weighed in stoichiometric ratios and mixed thoroughly in polythene bottles using zirconia balls in acetone medium for 3 h. The well mixed samples were dried and calcined at 1,250 °C for 4 h in an electrically heated furnace. The calcined powders were again ground well in agate mortar. A 5% solution of polyvinyl alcohol was added as binder to each powder, ground well and dried. Cylindrical pellets with diameter 14 mm and height 7 mm were made at 100 MPa pressure using a hydraulic press. The pellets were initially heated at a rate of 5 °C per minute up to 600 °C and soaked for an hour to expel the polyvinyl alcohol. Then the pellets were sintered in the temperature range 1,385–1,450 °C for 4 h. The cooling of the furnace in each case was carried out at a rate of 5 °C per minute.

The sintered pellets were polished well and densities were measured using Archimedes method. Small pellets were powdered well and X-ray diffraction (XRD) patterns were taken with X-ray Diffractometer (Philips Expert Pro) using CuKα radiation. Selected pellet was fine polished, thermally etched at 1,350 °C and Scanning Electron Micrograph (SEM) was taken using JEOL Model 6390 LV Scanning Electron Microscope. The Transmission Electron Microscopic (TEM) image and the corresponding SAED pattern were also taken using FEI Tecnai $30G^2$ S-TWIN transmission electron microscope operating at 300 kV. The dielectric constant (ε_r) and the unloaded quality factor ($Q_u \times f$) were then calculated using the computer interfaced network analyzer (Agilent 8753 ET) by the cavity resonator method. The specimen was placed at the centre of a cylindrical cavity whose size is 3–4 times greater than it. The microwave was coupled to the specimen and $TE_{01\delta}$ mode of resonance whose quality factor is intimately related to the dielectric loss was identified. The coefficient of thermal variation of resonant frequency (τ_f) over the range of temperature 20–80 °C was also measured. The FT-Raman spectra of the selected samples were recorded at room temperature over the wavenumber range 50–1,000 cm^{-1} using Bruker RFS 100/S spectrometer at a power level of 50 mW and at a resolution of 4 cm^{-1}. The samples were excited with a Nd:YAG laser lasing at 1,064 nm and the scattered radiations were detected using a standard Ge detector. The photoluminescence spectra were recorded using Perkin Elmer LS 55 Fluorescence Spectrometer.

3 Results and discussion

3.1 X-ray diffraction

The powder X-ray diffraction patterns of XTa_x ceramics are given in Fig. 1. The XRD patterns are indexed on the basis of $Ce_{0.5}Y_{0.5}NbTiO_6$ (JCPDS file No. 52-0384). The figure shows that XTa_x in which $x = 0$, 0.2, and 0.4 are prominently euxenite while those in which $x = 0.6$, 0.8, and 1 are prominently aeschynite in nature. There is a gradual change from euxenite character to aeschynite character as Ta is substituted for Nb. Selected area XRD patterns in the region $2\theta = 26$–31 for $x = 0.2$, 0.4 and 0.6 are given in Fig. 2. It helps to explain the change from the euxenite structure to aeschynite structure. Figure 2a is characteristic of euxenite structure and Fig. 2c is characteristic of aeschynite structure. The nature of Fig. 2b indicates the presence of both euxenite structure even though euxenite character is predominant as indicated by the τ_f value (−11.7 ppm/K). The intensity of the (112) peak at $2\theta = 30.4$ regularly increases from Fig. 2a–c, while that at $2\theta = 29.6$ decreases gradually. The (121) peak at $2\theta = 26.2$ which is characteristic of euxenite structure almost disappears in Fig. 2c.

3.2 Morphology

The SEM image of $XTa_{0.6}$ is given in Fig. 3. It reveals that the samples are well sintered. The particles are close packed with well defined boundaries and minimum porosity. Small particles of about 1 μm size and large

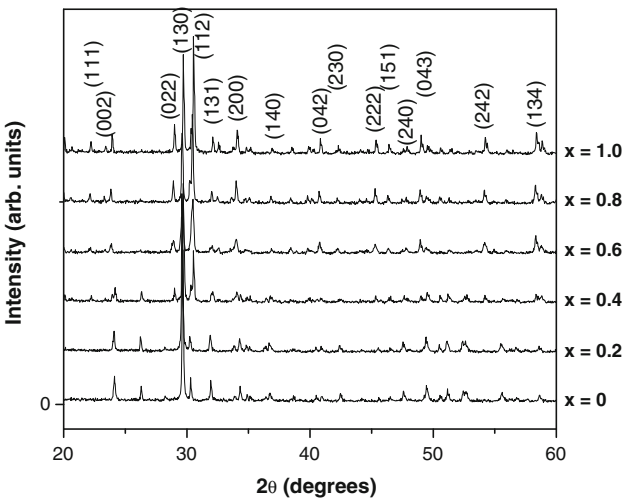

Fig. 1 XRD patterns of $(Sm_{0.5}Y_{0.5})Ti(Nb_{1-x}Ta_x)O_6$ ceramics

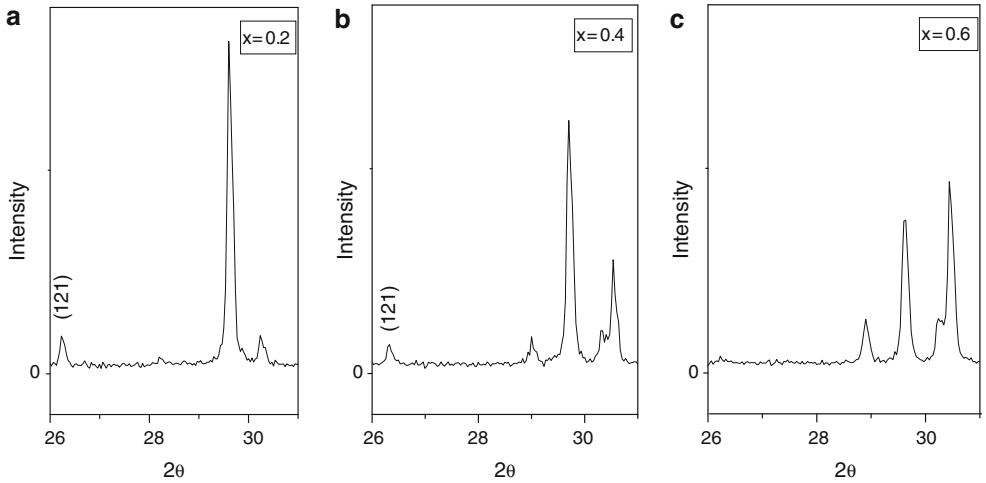

Fig. 2 XRD patterns in the region $2\theta = 26$–31 for **a** $XTa_{0.2}$, **b** $XTa_{0.4}$, and **c** $XTa_{0.6}$

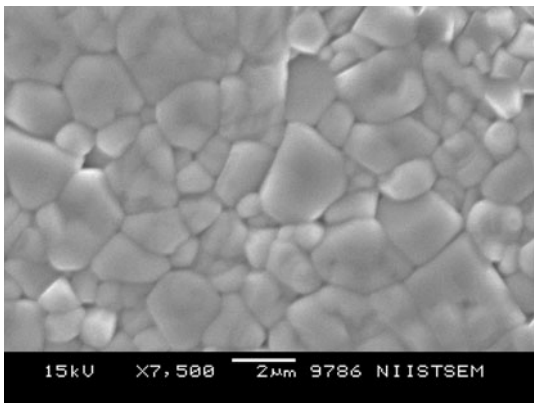

Fig. 3 SEM micrograph of $XTa_{0.6}$ ceramic

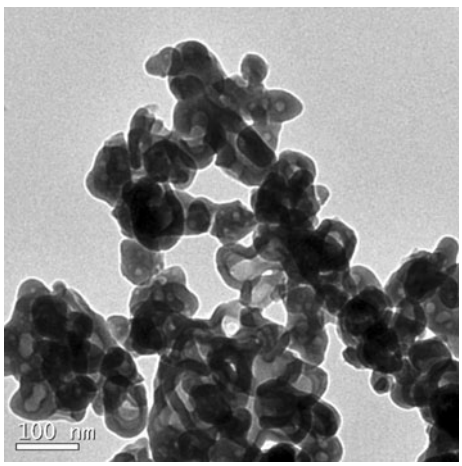

Fig. 4 TEM micrograph of $XTa_{0.6}$ ceramic

particles of about 4 μm size are observed showing the composite nature of the material. The TEM micrograph of $XTa_{0.6}$ is given in Fig. 4. It also shows two kinds of particles as shown by SEM.

3.3 Raman spectra

The FT Raman spectra of $XTa_{0.4}$ and $XTa_{0.6}$ recorded over the range 50–1,000 cm^{-1} is given in Fig. 5. The observed bands, their relative intensities and their assignments are given in Table 1. The factor group analysis of the parent materials $RETiNbO_6$ and $RETiTaO_6$ shows that 54 optical modes are expected in the Raman spectra of both the aeschynite and euxenite structures [15]. The spectra recorded in the present study show seven prominent peaks and several others that appear as very weak bands or as shoulders. The analysis of the spectral lines can be done on the basis of the characteristic vibrations of the Ta/Nb/TiO_6 octahedron. The octahedron with O_h symmetry has 15 internal modes that are distributed as, $\Gamma = A_{1g}$ (R) + E_g (R) + $2F_{1u}$ (IR) + F_{2g} (R) + F_{2u} (silent) [16].

The symmetric stretching mode of vibration υ_1 A_{1g} observed as a weak broad band with peaks at 869 and

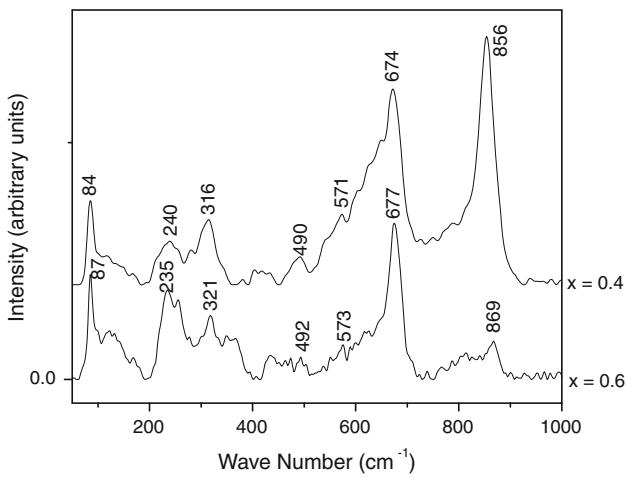

Fig. 5 Raman spectra of $XTa_{0.6}$ and $XTa_{0.4}$ ceramics

Table 1 Raman spectral data and band assignments of $XTa_{0.4}$ and $XTa_{0.6}$

$XTa_{0.4}$	$XTa_{0.6}$	Assignments
856 vs	869 w	υ_1 A_{1g}
	816 vw	
674 s	677 s	υ_2 E_g
649 sh	624 vw	
	614 vw	
571 w	596 vw	υ_3 F_{1u}
	573 w	
	546 vw	
490 w	492 vw	υ_4 F_{1u}
432 vw	475 vw	
420 vw	435 vw	
404 vw		
316 m	369 vw	υ_5 F_{2g}
	349 vw	
	321 m	
283 vw	282 vw	υ_6 F_{2u}
240 m	255 m	
	235 m	
170 vw	170 vw	Lattice vibrations
122 vw	135 vw	
84 s	122 vw	
	87 s	

vs, Very strong; s, strong; m, medium; w, weak; vw, very weak; sh, shoulder

816 cm^{-1} in $XTa_{0.6}$ has gained intensity and has shifted to 856 cm^{-1} in $XTa_{0.4}$. The asymmetric stretching υ_2 E_g observed as a strong band at 677 cm^{-1} in $XTa_{0.6}$ shows a red shift of 3 cm^{-1} in $XTa_{0.4}$. The symmetric bending mode υ_5 F_{2g} is observed as medium intensity band at 321 and 316 cm^{-1} in $XTa_{0.6}$ and $XTa_{0.4}$, respectively. The IR active F_{1u} modes, namely, the asymmetric stretching υ_3 F_{1u} and asymmetric bending υ_4 F_{1u} modes are observed as very weak bands in the Raman spectra in the regions 596–546 and 492–404 cm^{-1}, respectively. Weak or medium intense bands are observed in the region 283–235 cm^{-1}, which may be due to the silent mode υ_6 F_{2u}. The position and intensity of the spectral lines in $XTa_{0.6}$ are in good agreement with that of the bands of aeschynite structure and that of $XTa_{0.4}$ with that of the bands of euxenite structure as reported by Paschoal et al. [15]. This observation is in agreement with the XRD patterns, that $XTa_{0.4}$ has euxenite structure and $XTa_{0.6}$ has aeschynite structure.

3.4 Photoluminescence spectra

The photoluminescence spectra of the samples between the wavelengths 400 nm and 700 nm when excited at the wavelength 370 nm are given in Fig. 6. The photoluminescence spectra of XTa_x show emission lines at 413, 416, 424, 444, 460, 466, 484, 488, 492, 528, 555, 665, and 693 nm. The emission lines at 413 and 460 nm are assigned to $^4F_{2.5}$–$^4P^o_{2.5}$ and $^2G_{2.5}$–$^4P^o_{2.5}$, respectively of Ta. The emission lines at 416 and 424 are assigned to $^4D_{2.5}$–$^2D^o_{1.5}$ and $^4D_{2.5}$–$^2D^o_{2.5}$, respectively of Nb. The emission lines at 488 and 665 are assigned to $^3G_5$–$^3H^o_6$ and $^3F_2$–$^5G^o_3$, respectively of Ti. The emission lines at 444, 484, 492, and 693 nm are assigned to $^4F_{2.5}$–$^2F^o_{2.5}$, $^4F_{3.5}$–$^4F^o_{3.5}$, $^2P^o_1$–$^2S_{0.5}$, and $^2D_{2.5}$–$^4F^o_{1.5}$, respectively of Y. The emission lines at 466, 528, and 555 nm are assigned to $^7F_5$–$^0A^o_4$, $^7F_6$–$^7F^o_6$, and $^7F_3$–$^7F^o_3$, respectively of Sm.

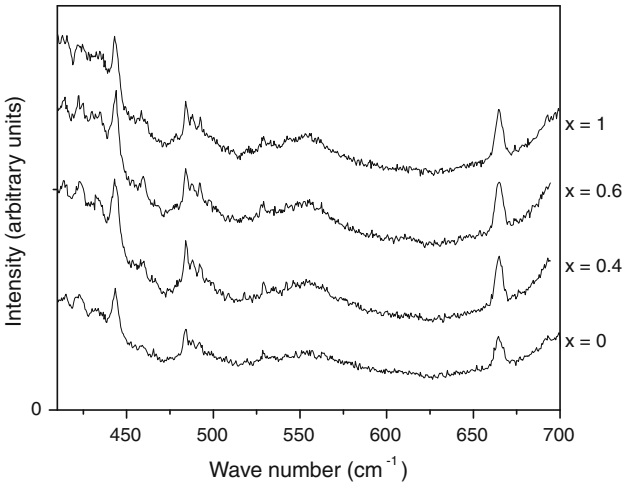

Fig. 6 PL spectra of XTa_x ceramics

3.5 Microwave dielectric properties and densities

The microwave dielectric properties of XTa_x ceramics are given in Table 2. Sebastian et al. [13] have reported sintering temperatures of 1,360 °C for $SmTiNbO_6$ and 1,400 °C for $YTiNbO_6$. The composite $Sm_{0.5}Y_{0.5}TiNbO_6$ was sintered at an optimum temperature of 1,385 °C with 95% densification. Surendran et al. [14] have reported sintering temperatures of 1,500 °C for $SmTiTaO_6$ and 1,625 °C for $YTiTaO_6$. The composite $Sm_{0.5}Y_{0.5}TiTaO_6$ was sintered at a lower temperature of 1,450 °C with 97% densification. As the amount of tantalum is increased there is a regular increase in the density. The variation of ε_r and τ_f with the bulk densities of the samples is given in Fig. 7. The densities increase proportionally with the increase in Ta concentration. For Ta substituted compositions $XTa_{0.2}$, $XTa_{0.4}$, $XTa_{0.6}$ and $XTa_{0.8}$ the ε_r and τ_f increase with respect to the increase in concentration of Ta. For the end compositions, XTa_0 and XTa_1, there is a slight change from the normal variation. This may be due to the stabilization of these compositions in comparison with the solid solutions of Nb and Ta.

Table 2 Microwave dielectric properties of XTa_x ceramics

x	Sintering temp. (°C)	D (mm)	L (mm)	Frequency (GHz)	ε_r	τ_f (ppm/°C)	$Q_u \times f$ (GHz)
0	1,385	12.27	7.46	5.01	22.3	−37.1	8,760
0.2	1,400	12.16	7.49	5.14	21.5	−41.5	13,120
0.4	1,400	12.11	7.25	4.54	28.1	−11.7	12,520
0.6	1,400	12.02	7.06	4.06	35.0	+7.2	8,920
0.8	1,425	11.94	6.86	4.14	35.3	+9.7	10,640
1.0	1,450	11.90	6.76	4.30	33.0	+3.8	14,930

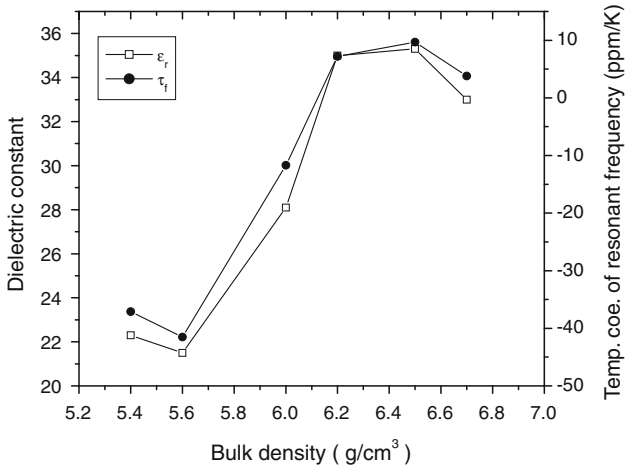

Fig. 7 Variation of ε_r and τ_f of XTa_x ceramics with bulk density

4 Conclusion

The compositions in which x is greater than 0.2 satisfy all the essential requirements of a dielectric resonator, viz., high dielectric constant, low temperature coefficient of resonant frequency and high quality factor. A ceramic with zero τ_f is expected in between the compositions $x = 0.4$ and $x = 0.6$. The SEM micrographs show that the samples are well sintered with minimum porosity. The samples are Raman active and the Raman spectra are used to confirm the structure. The samples also show photo luminescent properties. Hence these compositions are suitable for dielectric resonator and ceramic laser applications.

Acknowledgments We would like to express our sincere gratitude to Dr. M.T. Sebastian for his help in microwave measurements. Dr. Sam Solomon acknowledges University Grants Commission for the post doctoral research award.

References

1. R.D. Richtmyer, J. Appl. Phys. **10**, 391 (1939)
2. R.J. Cava, J. Mater. Chem. **11**, 54 (2001)
3. S. Solomon, Manoj Kumar, K.P. Surendran, M.T. Sebastian, P. Mohanan, Mater. Chem. Phys. **67**, 291 (2001)
4. T. Oishi, A. Khan, H. Ohsato, H. Ogawa, J. Eur. Ceram. Soc. **26**, 2489 (2003)
5. L. Fang, H. Zhang, X.K. Hong, F.C. Merg, J.F. Yang, T.H. Huang, Mater. Lett. **58**, 3884 (2004)
6. H. Padmakumar, J.K. Thomas, M.R. Varma, S. Solomon, J. Alloys Compd. **455**, 475–479 (2008)
7. K.P. Surendran, P. Mohanan, M.T. Sebastian, J. Eur. Ceram. Soc. **23**, 2489 (2003)
8. S. Solomon, J.T. Joseph, H. Padmakumar, J.K. Thomas, Mater. Lett. **60**, 2814–2818 (2006)
9. C.-L. Huang, H.-L. Chen, C.-C. Wu, Mater. Res. Bull. **36**, 1645–1652 (2001)
10. J.T. Joseph, H. Padmakumar, M.R. Varma, J.K. Thomas, S. Solomon, Mater. Lett. **62**, 1064–1066 (2008)
11. X. Liu, F. Gao, C. Tian, Mater. Res. Bull. **43**, 693 (2008)
12. H. Padmakumar, J.T. Joseph, J.K. Thomas, K. Joy, S. Solomon, J. Mater. Sci.: Mater. Electron. **20**(6), 551–554 (2009)
13. M.T. Sebastian, S. Solomon, R. Ratheesh, J. George, P. Mohanan, J. Am. Ceram. Soc. **84**(7), 1487–1489 (2001)
14. K.P. Surendran, S. Solomon, M.R. Varma, P. Mohanan, M.T. Sebastian, J. Mater. Res. **17**(10), 2561–2566 (2002)
15. C.W.A. Paschoal, R.L. Moreira, C. Fantini, M.A. Pimenta, K.P. Surendran, M.T. Sebastian, J. Eur. Ceram. Soc. **23**, 2601–2666 (2003)
16. R. Ratheesh, H. Sreemoolanadhan, M.T. Sebastian, J. Solid, State Chem. **131**, 2–8 (1997)